

Degradation of Anionic Dye (Acid Orange II) by Bentonite Supported Nano-Zero Valent Iron

N.A. ZARIME*, W.Z. WAN YAACOB and H. JAMIL

Geology Programme, School of Environmental Sciences and Natural Resources, Faculty of Science and Technology, Universiti Kebangsaan Malaysia, 43600 Bangi, Selangor, Malaysia

*Corresponding author: E-mail: aishahzarime@gmail.com; drwzwy@gmail.com

Received: 31 December 2018;

Accepted: 15 February 2019;

Published online: 29 April 2019;

AJC-19373

The nano-zero valent iron (nZVI) has been reported as an excellent material to decolourize the anionic dyes. Aggregation of nZVI tends to reduce its reactivity. Due to this reason, modifications of nZVI were applied by using bentonite. Bentonite supported nano-zero valent irons (B-nZVI) was synthesized by using reduction method of ferrous ions and sodium borohydride in presence of bentonite. The objective of this study was to evaluate the performance of composite nanoscale zero-valent iron (nZVI) in decolorized of acid orange II from aqueous solutions. All the three adsorbent materials (nZVI, B-nZVI and bentonite) were characterized by physical, chemical, mineralogical and morphological properties such as Brunnaer-Emmett-Teller (BET) surface area, X-ray photoelectron spectroscopy with auger electron spectroscopy (XPS-AES), field emission scanning electron microscopy (FESEM) and X-ray diffraction (XRD). The batch adsorption tests for all adsorbent materials have been conducted to determine the effectiveness of both materials in dye removal. The five effects have been analyzed in Batch test among others concentration, dose, pH, kinetic and temperature. The study found in all effects, B-nZVI ($q_{e\text{ opt}} = 8.9286$ mg/g) showed the higher adsorption capacity followed by nZVI ($q_{e\text{ opt}} = 8.1224$ mg/g) and bentonite ($q_{e\text{ opt}} = 5.8469$ mg/g). The effectiveness of B-nZVI was due to the dispersion of nZVI particles bentonite particles, consequently provided more sites for adsorption. This study discovered that B-nZVI has a high potential to be a low-cost adsorbent for decolorized anionic dye from synthetic dye wastewater.

Keywords: Acid orange II, Bentonite, Composite nano zero valent iron, Batch test.

INTRODUCTION

Azo dye is commonly used in texture industry and it becomes an environmental worldwide issue. According to several authors [1-4], azo dyes create the complex aromatic structures that highly resistant to microorganisms and defiant to conventional biological wastewater treatment processes which at the end will initiate significant burden on nature environment. Acid orange II (4-(2-hydroxy-1-naphthylazo)-benzenesulfonic acid sodium) is an anionic azo dye which is non-biodegradable in nature and proven to induce cytogenetical changes in animals [5,6].

Various ways of treatment have been applied to remove hazardous chemical from dyes. One of them is nanoscale zero-valent iron (nZVI). The nZVI is a new generation of environmental remediation technology that provides cost-effective solutions to the environmental remediation problems [7]. However, the nZVI can easily aggregate due to strong van der

Waals forces. Prior research, modification on nZVI particle surface proposed the use of clay materials to prevent the particles from aggregation [8-10]. In this research, iron nanoparticles were synthesized using bentonites. Bentonite has a low permeability due to its small pore sizes, complex porous structures and a high specific surface area which allow for strong physico-chemical interactions to occur between fluids and dissolved species [11]. The main objective of the current study was to investigate the effectiveness of bentonite supported nanoparticles in decolourizing the anionic dye, acid orange II.

EXPERIMENTAL

Bentonite was purchased from R&M Chemicals. Acid orange II has been supplied in a solid state with high purity (wt. % 99.9 %) from Tianjin Yuhua Co., China. For synthesis of composite nZVI, ferric chloride tetrahydrate ($\text{FeCl}_3 \cdot 6\text{H}_2\text{O}$, Acros Organics, 99 + %), sodium borohidrat (NaBH_4 , Acros

Organics, 98 + %) and ethanol (Fisher Scientific, 99.4 %) were used in this analysis.

Synthesis of nanoparticles: Bentonite supported nano zero valent iron (B-nZVI) was synthesized using a chemical reduction method [7,10]. Ferric chloride solutions were prepared by dissolving 4.38 g ferric chloride tetrahydrate with 50 mL mixture of ethanol and deionized water (35 mL ethanol + 15 mL of deionized water). Bentonite was added to ferric chloride solution and the mixture was shaken using an ultrasonic shaker for 30 min. To produce NaBH₄ solutions, 6.091 g of sodium borohydride, NaBH₄ were dissolved in 100 mL deionized water. The NaBH₄ solutions were pipetted and dropped (1-2 drop per second) into ferric chloride solution on a magnetic stirrer. The mixture was then stirred for 20 min. The black particles were filtered and washed using ethanol (50 mL) for three times. The black particles were oven dried at 50 °C for about 12 h.

Characterization of nanoparticles: The physical characterization supported nanoparticles was analyzed using Brunauer-Emmett-Teller by N₂ desorption method to determine the specific area of particles. Chemical characterization was conducted using X-ray photoelectron spectroscopy and auger electron spectroscopy (XPS-AES) to measure the surficial chemical composition and element valence of particles. The morphology and mineralogy of the particles were also characterized using field emission scanning electron microscope (FESEM) and X-ray diffraction (XRD).

Batch test: Batch test method was applied as reported by USEPA [12]. The supported nanoparticle materials were prepared by passing through 63 µm sieve. Acid orange II solution was prepared with 7 different concentrations namely 5, 20, 40, 60, 80, 100 and 150 mg/L. To perform batch test, 0.5 g of B-nZVI with 50 mL of acid orange II (1:100 ratio soil/solution) was mixed in centrifuge tubes. The mixture samples were shaken at 150 rpm for 3 h to attain their equilibrium. After shaken, mixture samples were centrifuged at 1500 rpm for 15 min and filtered through 45 µm nitrocellulose membranes. The solutions were analyzed using UV-visible spectrophotometer (UV1201). Batch test analysis included 5 parameters that were dose, concentration pH, kinetic and temperature. To determine the optimum dosage, the different dosages materials (0.03, 0.05, 0.07, 0.1, 0.3, 0.5, 0.7 and 1.0 g) were used. In this case, different dosages were added to 50 mL acid orange II (50 mg/L). The concentration effect was performed using 5, 20, 40, 60, 80, 100 and 150 mg/L of acid orange II while for pH effect, different pH levels of acid orange II (pH 2, 4, 6, 8, 10 and 12) were determined and made use. Kinetic effect was represented by shaking times (5, 10, 20, 30, 45, 60, 120, 180 and 360 min) while for temperature effect, different temperatures (30, 40, 50 and 60 °C) were used in this analysis. For all factors, the batch test analysis was carried out with the ratio 1:100.

Adsorption isotherm: In this study, adsorption data were analyzed using linear equations. The concentration of acid orange II adsorbed by particles, q_e was calculated as follows:

$$q_e = \frac{(C_o - C_e)V}{M}$$

where; C_o and C_e representing initial concentration and equilibrium concentration respectively (mg/L), V is a volume of solution added (mL), M is mass of air-dried material (g).

RESULTS AND DISCUSSION

Particle characterization: Table-1 shows the physical characterization, which is Brunauer-Emmett-Teller specific surface area (BET) for bentonite, nZVI and B-nZVI. It was observed that bentonite has the highest surface area (74.78 m²/g) followed by B-nZVI (5.64 m²/g) and nZVI (1.5724 m²/g). Bentonite also has the highest pore volume (0.0994 m³/g) followed by B-nZVI (0.0226 m³/g) and nZVI (0.0042 cm³/g). B-nZVI has intermediate pore volume value due to the fact that nZVI particles were filling into bentonite pores [8,13]. The chemical characterization of X-ray photoelectron spectroscopy with auger electron spectroscopy (XPS-AES) for all samples were presented in Fig. 1. In Fig. 1a, it was shown that nZVI has Na, Fe, O, C and B elements on its particles surface while bentonite (Fig. 1c) and B-nZVI (Fig. 1e) have Na, Fe, O, Ca, C, Si, Al, Mg and Na, Fe, O, Ca, C, B, Si, Al, Mg; respectively on their particles surface. Carbon was spotted in all samples as a result of carbon coating and using adhesive carbon tape [6]. According to Yaacob and How [10], B elements presented due to NaBH₄ that has been used to synthesize nanoparticles. The elements of Na, Al, Mg, Ca and Si were found on bentonite and B-nZVI as this clay mineral has two siloxane tetrahedral sheets with an aluminium octahedral sheet, 2:1 structure [6]. To confirm the occurrence of Fe, the XPS-AES spectrum of the Fe 2p were illustrated in Fig. 1b, Fig. 1d and Fig. 1f. For nZVI (Fig. 1b), binding energies for (Fe₂O₃) and Fe 2p_{3/2} (Fe₃O₄) were 723.0 eV and 708.0 eV; respectively while for B-nZVI (Fig. 1f), the peak of Fe 2p_{1/2} (Fe₂O₃) and Fe 2p_{3/2} (Fe₃O₄) exhibited the binding energy at 724.0 eV and 710.0 eV; respectively. For both nZVI and B-nZVI, small peaks at 706.1 eV and 719.7 eV were corresponding to zero valent iron (Fe⁰ 2p_{3/2} and Fe⁰ 2p_{1/2} respectively) [10]. From the Fig. 1d, it was noted that bentonite binding energy for Fe 2p_{1/2} (Fe₂O₃) and Fe 2p_{3/2} (Fe₃O₄) were 723.0 eV and 710.0 eV; respectively.

TABLE-1
BRUNAUER-EMMETT-TELLER SURFACE AREA (BET)
RESULTS FOR ABSORBENT MATERIALS

Sample	BET surface area (m ² /g)	Pore volume (cm ³ /g)	Pore size (Å)
nZVI	1.5724	0.0042	107.0115 (10.70115 nm)
Bentonite	74.7755	0.0994	53.1595 (5.31595 nm)
B-nZVI	5.6418	0.0226	160.2891 (16.02891 nm)

Fig. 2 displays the morphology and textures (shape and size) of the nanoparticles by using field emission scanning electron microscopy (FESEM) analysis. Fig. 2a and Fig. 2b illustrate the nZVI particles in which it has spherical shapes (ranging from 54.75 nm to 71.46 nm) and aggregated into a chain-like [14,15]. According to Xi *et al.* [6] and Han *et al.* [16], nZVI particles were aggregated due to magnetostatic attraction and huge interface energy between the iron particles. In Fig. 2c, it was shown that bentonite has flaky and irregular shapes (curled and crumpled structures). While in Fig. 2c and Fig. 2d, B-nZVI confirmed the nZVI spherical particles (ranging between 41.91 nm to 4.88 nm), embedding and dispersing well in flaky and irregular shapes of bentonites. Bentonite presented as a media to prevent aggregation of zero valent

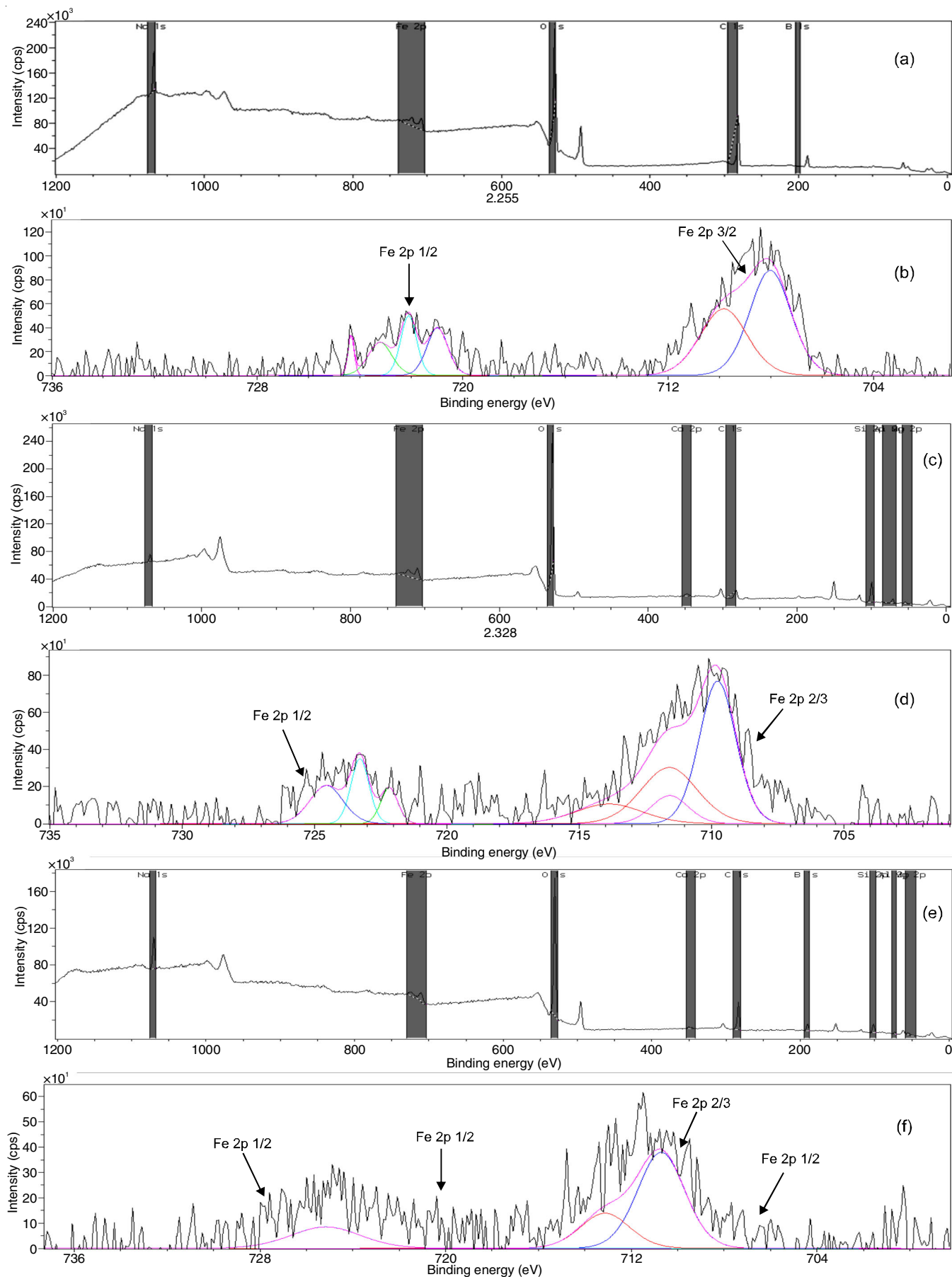


Fig. 1. X-ray photoelectron spectroscopy with Auger electron spectroscopy (XPS-AES) of (a) nZVI, (b) nZVI Fe 2p line, (c) Bentonite, (d) Bentonite Fe 2p line, (e) B-nZVI and (f) B-nZVI Fe 2p line

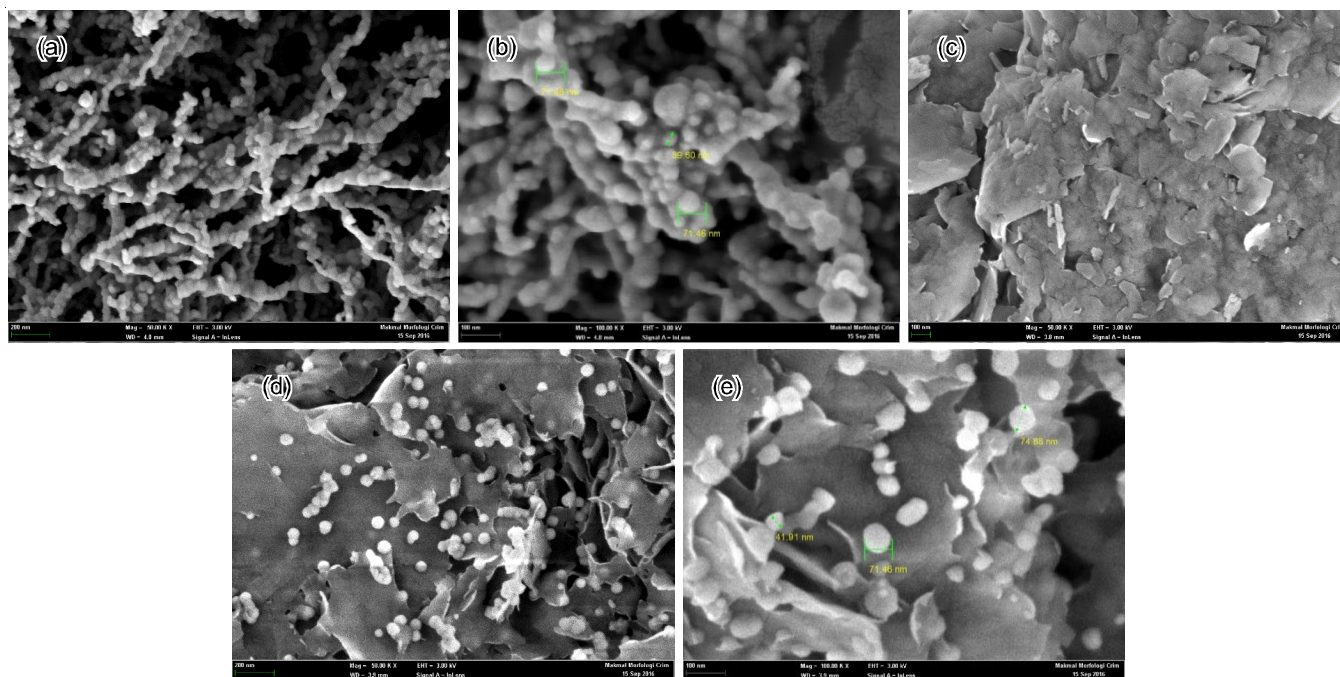


Fig. 2. Field emission scanning electron microscopy (FESEM) images for (a) nZVI, magnification: 50000X, (b) nZVI, magnification: 100000X, (c) Bentonite, magnification: 50000X, (d) B-nZVI, magnification: 50000X and (e) B-nZVI, magnification: 100000X

iron, thus, providing more sites for adsorbing dyes in wastewater. The XRD patterns of nZVI, bentonite and B-nZVI were shown in Fig. 3. Through this analysis, the FeO (α -FeO) at the peak of $2\theta = 44.67^\circ$ in nZVI and B-nZVI sample was found to be corresponding to the formation of nano zero valent iron. The peak of $2\theta = 5.8719^\circ$ represented montmorillonite in bentonite sample.

Batch test

Effect of adsorbent dosage: Fig. 4 explains the results of dose effect on acid orange II by adsorbent materials (nZVI, bentonite and B-nZVI). The curve delineated that B-nZVI adsorbed more dye followed by nZVI and bentonites. Higher adsorption capacity of B-nZVI was due to a larger specific

area and the availability of more adsorption sites to accelerate initial reaction [10,17,18]. The results also illustrated that adsorption capacity for all materials decreased with the increasing dosage of adsorbent materials. According to Veli and Alyüz [19], increasing of dosage will cause the aggregation of particles to decrease the surface area of adsorbent materials and increase the diffusion path length of pollutant/dye. As the concentration of dye was low, the increment of dosage resulting in unsaturation adsorption sites and nZVI particles were oxidized to Fe_2O_3 and Fe_3O_4 , hence, the adsorption capacity of adsorbent materials decreased when the dosage reached a certain level. The optimum adsorbent dosage was 0.5 g and further experiments were carried out using this dose.

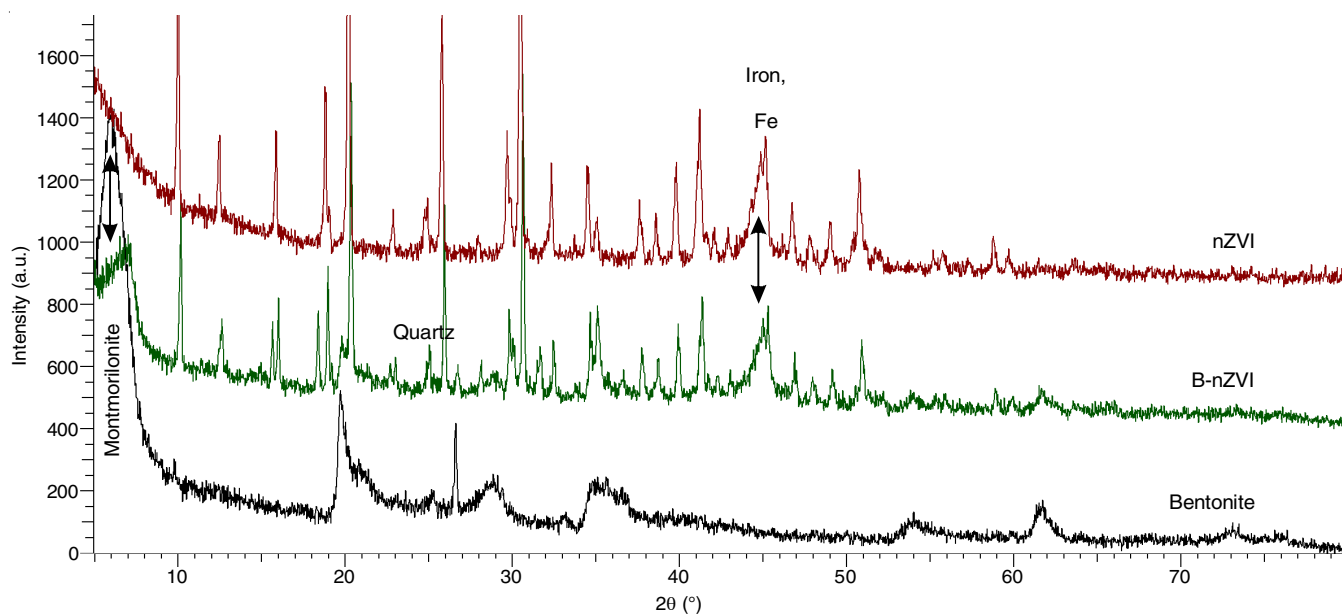


Fig. 3. XRD patterns for bentonite, nZVI and B-nZVI

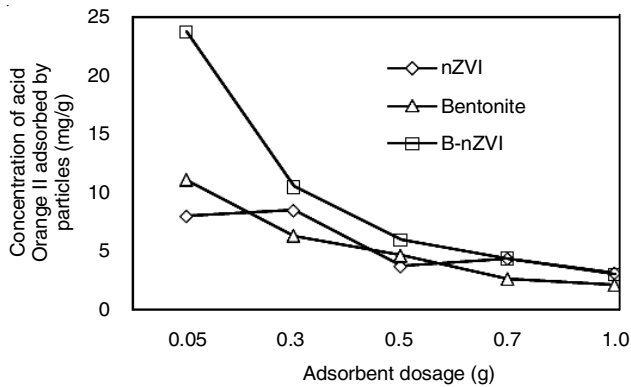


Fig. 4. Effect of adsorbent dosage of nZVI, bentonite and B-nZVI

Effect of initial concentration: The effect of initial concentration of acid orange II were studied over the concentration ranged from 5 to 150 mg/L. The result was presented in Fig. 5 and it was shown that the adsorption capacity increased with the increment of initial concentration until at one point it became constant although the initial concentration increased. The B-nZVI ($q_{e\text{ opt}} = 8.9286$ mg/g) showed a higher adsorption capacity followed closely by nZVI ($q_{e\text{ opt}} = 8.1224$ mg/g) and bentonite ($q_{e\text{ opt}} = 5.8469$ mg/g). The optimum concentration has been determined to be 40 mg/L as the graph started to be constant and indicating adsorbent materials was saturated with dye. In this condition, no more dye or metal ions can be adsorbed [19].

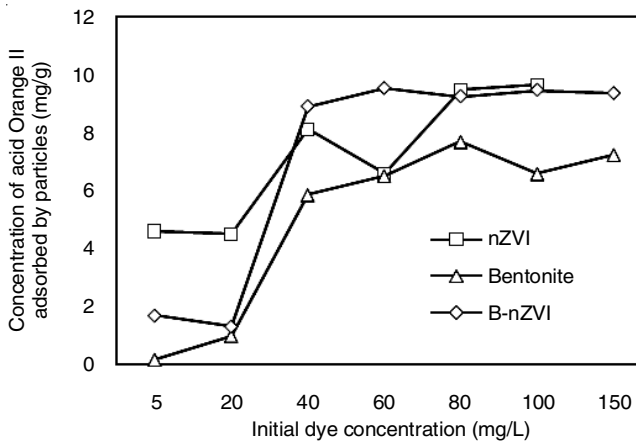


Fig. 5. Effect of dye initial concentration on adsorption capacity

Effect of initial pH: The dye wastewater has a wide range of pH values. In this study, the effect of initial pH in decolorizing acid orange II has been assessed and presented in Fig. 6. Fig. 6 illustrates that nZVI ($q_{e\text{ pH } 2} = 10.3349$ mg/g) and B-nZVI ($q_{e\text{ pH } 2} = 10.2698$ mg/g) have the highest adsorption capacity compared with bentonite ($q_{e\text{ pH } 2} = 0.574$ mg/g). As reported by Luo *et al.* [20], the core shell of nZVI possessed hydroxyl groups when it interfaced with dye solution and it has its own capability to immobilize sorbate molecules by surface complexation. The nZVI core also formed an electron where it could reduce acid orange II. The pH 2 was selected as the optimum pH as it showed the maximum adsorption. According to Kakavandi *et al.* [21] and Chang *et al.* [22], the maximum adsorption was in acidic condition due to the electrostatic attraction between positive charged surface of the adsorbent and the anionic dye. As pH of dye increased, negative

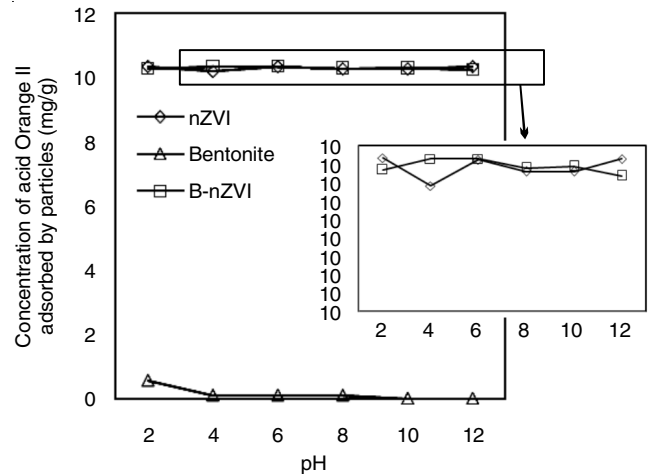


Fig. 6. Effect of initial pH acid orange II using nZVI, bentonite and B-nZVI

charged sites were also increased. Negative charge on the adsorbent's surface site did not favour the adsorption of ionic dye due to electrostatic repulsion. There was an adsorption competition between OH^- ions and anionic at higher pH levels, resulting a lower adsorption capacity [22,23].

Effect of time: The effect of contact time (kinetic) on the decolorization of acid orange II was illustrated in Fig. 7. It was observed that nZVI ($q_{e\text{ 5 min}} = 6.8607$ mg/g) has highest adsorption capacity followed by B-nZVI ($q_{e\text{ 5 min}} = 6.7262$ mg/g) and bentonite ($q_{e\text{ 5 min}} = 0.3228$ mg/g). All curves showed higher adsorptions at the beginning and remained constant (reached equilibrium) after 5 min. Rapid phase at 0 to 5 min was due to the presence of large number of vacant sites, which led to the increase of concentration gradient between dye solution and adsorbent surface [24].

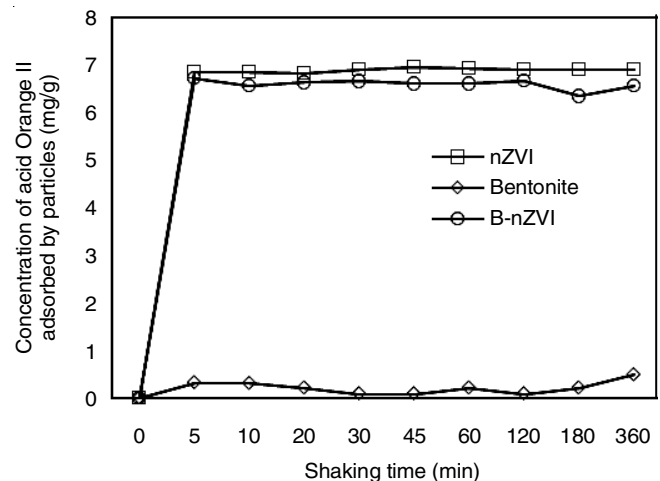


Fig. 7. Effect of shaking time in adsorption capacity of nZVI, bentonite and B-nZVI

Effect of temperature: To assess the effect of different temperatures, batch experiments were conducted at 30, 40, 50 and 60 °C with 50 mg/L dye concentration and 0.5 g adsorbent dosage. The results were displayed in Fig. 8. From the graph, nZVI ($q_e = 5.6819$ mg/g) and B-nZVI ($q_e = 5.6819$ mg/g) curves were constant and the adsorption capacity was higher compared with bentonite ($q_e = 0.2977$ mg/g). Composite nanoparticles provided both mineral and nZVI particles surfaces for greater

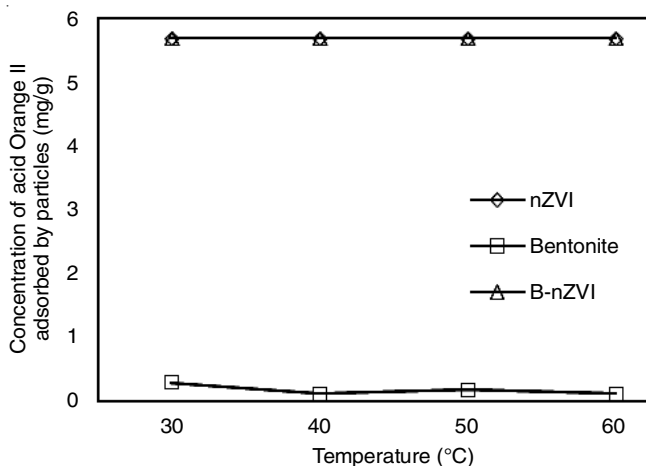


Fig. 8. Effect of temperature in adsorption capacity of nZVI, bentonite and B-nZVI

adsorption sites compared with bentonite itself. The graph also showed the temperature effect did not give any significant effect on nZVI and B-nZVI. For bentonite, the adsorption capacity of acid orange II was slightly higher at a temperature of 30 °C ($q_e = 0.2977$ mg/g) compared with other temperature. Through this temperature effect, it was proved that composite nanoparticles were stable towards any temperature and it suggested the best material for water treatment in the natural environment.

Conclusion

In the present study, bentonite supported nano-zero valent iron was successfully synthesized using chemical reduction method. Through characterization method, results demonstrated that B-nZVI has the ability to prevent the oxidation and aggregation of nano-zero valent iron particles. B-nZVI also showed the highest adsorption capacity of acid orange II, followed by nZVI and bentonite. The optimum condition for the adsorption process was obtained at 0.5 g of absorbent dosage, 40 mg/L initial concentration, acidic pH (pH = 2), the contact time of 5 min and there was no significant effect on temperature for composite nanoparticles. As bentonite can easily be obtained at a low-cost, B-nZVI was the best prospect to remediate the anionic dye in wastewater.

ACKNOWLEDGEMENTS

This research project was supported by Centre for Research & Instrumentation Management (CRIM), UKM with a financial support from Ministry of Education. Authors acknowledged Geology Program, Faculty of Science and Technology, Universiti Kebangsaan Malaysia (UKM), Malaysia for their assistance in conducting this research.

CONFLICT OF INTEREST

The authors declare that there is no conflict of interests regarding the publication of this article.

REFERENCES

- H.-Y. Shu, C.-R. Huang and M.-C. Chang, *Chemosphere*, **29**, 2597 (1994); [https://doi.org/10.1016/0045-6535\(94\)90060-4](https://doi.org/10.1016/0045-6535(94)90060-4).
- B. Manu and S. Chaudhari, *Process Biochem.*, **38**, 1213 (2003); [https://doi.org/10.1016/S0032-9592\(02\)00291-1](https://doi.org/10.1016/S0032-9592(02)00291-1).
- U. Pagga and D. Brown, *Chemosphere*, **15**, 479 (1986); [https://doi.org/10.1016/0045-6535\(86\)90542-4](https://doi.org/10.1016/0045-6535(86)90542-4).
- C. Zhang, Z. Zhu, H. Zhang and Z. Hu, *J. Environ. Sci.*, **24**, 1021 (2012); [https://doi.org/10.1016/S1001-0742\(11\)60894-2](https://doi.org/10.1016/S1001-0742(11)60894-2).
- O. Prasad and P. Rastogi, *Experientia*, **38**, 1240 (1982); <https://doi.org/10.1007/BF01959764>.
- Y. Xi, M. Megharaj and R. Naidu, *Appl. Clay Sci.*, **53**, 716 (2011); <https://doi.org/10.1016/j.clay.2011.06.010>.
- Y. Zou, X. Wang, A. Khan, P. Wang, Y. Liu, A. Alsaedi, T. Hayat and X. Wang, *Environ. Sci. Technol.*, **50**, 7290 (2016); <https://doi.org/10.1021/acs.est.6b01897>.
- Z. Chen, Y. Cheng, Z. Chen, M. Megharaj and R. Naidu, *J. Nanopart. Res.*, **14**, 899 (2012); <https://doi.org/10.1007/s11051-012-0899-0>.
- G. Cheng, H. Jia, H. Li, B.J. Teppen and S.A. Boyd, *Environ. Sci. Technol.*, **44**, 11 (2010); <https://doi.org/10.1021/es903305p>.
- W.Z.W. Yaacob and H.K. How, *Am. J. Environ. Sci.*, **11**, 115 (2015); <https://doi.org/10.3844/ajessp.2015.115.124>.
- J. Cuevas, A.I. Ruiz, I.S. de Soto, T. Sevilla, J.R. Procopio, P. Da Silva, M.J. Gismera, M. Regadío, N. Sánchez Jiménez, M. Rodríguez Rastrero and S. Leguey, *J. Environ. Manage.*, **95**, S175 (2012); <https://doi.org/10.1016/j.jenvman.2011.02.014>.
- USEPA, Batch-Type Procedures for Estimating Soil Adsorption of Chemicals, EPA/530/SW- 87/006-F (1992).
- H. Zhu, Y. Jia, X. Wu and H. Wang, *J. Hazard. Mater.*, **172**, 1591 (2009); <https://doi.org/10.1016/j.jhazmat.2009.08.031>.
- D.V. Kerkez, D.D. Tomasevic, G. Kozma, M.R. Bečić-Tomin, M.D. Prica, S.D. Rončević, Á. Kukovec, B.D. Dalmacija and Z. Kónya, *J. Taiwan Inst. Chem. Eng.*, **45**, 2451 (2014); <https://doi.org/10.1016/j.jtice.2014.04.019>.
- L. Shi, X. Zhang and Z. Chen, *Water Res.*, **45**, 886 (2011); <https://doi.org/10.1016/j.watres.2010.09.025>.
- L. Han, S. Xue, S. Zhao, J. Yan, L. Qian and M. Chen, *PLoS One*, **10**, e0132067 (2015); <https://doi.org/10.1371/journal.pone.0132067>.
- M.C. Somasekhara Reddy, L. Sivaramakrishna and V. Reddy, *J. Hazard. Mater.*, **203-204**, 118 (2012); <https://doi.org/10.1016/j.jhazmat.2011.11.083>.
- H. Shu, M. Chang, C. Chen and P. Chen, *J. Hazard. Mater.*, **184**, 499 (2010); <https://doi.org/10.1016/j.jhazmat.2010.08.064>.
- S. Veli and B. Alyüz, *J. Hazard. Mater.*, **149**, 226 (2007); <https://doi.org/10.1016/j.jhazmat.2007.04.109>.
- S. Luo, P. Qin, J. Shao, L. Peng, Q. Zeng and J. Gu, *Chem. Eng. J.*, **223**, 1 (2013); <https://doi.org/10.1016/j.cej.2012.10.088>.
- B. Kakavandi, R.R. Kalantary, M. Farzadkia, A.H. Mahvi, A. Esrafil, A. Azari, A.R. Yari and A.B. Javid, *J. Environ. Health Sci. Eng.*, **12**, 115 (2014); <https://doi.org/10.1186/s40201-014-0115-5>.
- H.-S. Chang, K.-H. Choo, B. Lee and S.-J. Choi, *J. Hazard. Mater.*, **172**, 1 (2009); <https://doi.org/10.1016/j.jhazmat.2009.06.135>.
- M. Arami, N.Y. Limaee, N.M. Mahmoodi and N.S. Tabrizi, *J. Colloid Interface Sci.*, **288**, 371 (2005); <https://doi.org/10.1016/j.jcis.2005.03.020>.
- S. Shahmohammadi-Kalalagh, H. Babazadeh, A.H. Nazemi and M. Manshouri, *Caspian J. Environ. Sci.*, **9**, 2 (2011).